Neuregulin/ErbB regulate neuromuscular junction development by phosphorylation of α-dystrobrevin

Nadine Schmidt,[1] Mohammed Akaaboune,[2] Nadesan Gajendran,[1] Isabel Martinez-Pena y Valenzuela,[2] Sarah Wakefield,[1] Raphael Thurnheer,[3] and Hans Rudolf Brenner[1]

[1]Institute of Physiology, Department of Biomedicine, University of Basel, CH-4056, Basel, Switzerland
[2]Department of Molecular, Cellular, and Developmental Biology and Program in Neuroscience, University of Michigan, Ann Arbor, MI 48109
[3]Departments of Anesthesia and Biomedicine, Basel University Hospital, CH-4031 Basel, Switzerland

Neuregulin (NRG)/ErbB signaling is involved in numerous developmental processes in the nervous system, including synapse formation and function in the central nervous system. Although intensively investigated, its role at the neuromuscular synapse has remained elusive. Here, we demonstrate that loss of neuromuscular NRG/ErbB signaling destabilized anchoring of acetylcholine receptors (AChRs) in the postsynaptic muscle membrane and that this effect was caused by dephosphorylation of α-dystrobrevin1, a component of the postsynaptic scaffold. Specifically, in mice in which NRG signaling to muscle was genetically or pharmacologically abolished, postsynaptic AChRs moved rapidly from the synaptic to the perisynaptic membrane, and the subsynaptic scaffold that anchors the AChRs was impaired. These defects combined compromised synaptic transmission. We further show that blockade of NRG/ErbB signaling abolished tyrosine phosphorylation of α-dystrobrevin1, which reduced the stability of receptors in agrin-induced AChR clusters in cultured myotubes. Our data indicate that NRG/ErbB signaling maintains high efficacy of synaptic transmission by stabilizing the postsynaptic apparatus via phosphorylation of α-dystrobrevin1.

Introduction

Neuregulins and their effectors, the ErbBs, are major factors involved in the function of central and peripheral synapses. Their mode of action has remained elusive, however. At the neuromuscular junction (NMJ) NRG1 from motor neurons activating ErbB receptors in muscle has been proposed to control *achr* subunit gene expression from subsynaptic muscle nuclei (Schaeffer et al., 2001). However, mice in which NRG/ErbB signaling to muscle is prevented by abolishment of *erbb2* and *erbb4* genes selectively in muscle nonetheless express synaptic *achr* genes at almost normal levels (Escher et al., 2005). Thus, the function of NRG1/ErbB signaling at the NMJ has remained unknown to this date. The present work is aimed at elucidating this function.

At the mature NMJ, the density of acetylcholine receptors (AChRs) is determined by an equilibrium between the insertion of receptors into, and their removal from, the postsynaptic membrane. Like synaptic receptors in the central nervous system, AChRs can shuttle between synaptic and nonsynaptic zones (Akaaboune et al., 2002). Once internalized, the AChRs are not simply degraded. A significant number of internalized receptors are recycled back into the postsynaptic membrane in a manner that depends on muscle activity (Bruneau et al., 2005a; 2009, Bruneau and Akaaboune, 2006).

The maturation and maintenance of the postsynaptic membrane at the NMJ are tightly controlled by the dystrophin glycoprotein complex. For example, synapses deficient in α-dystrobrevins (α-DB), a component of the postsynaptic apparatus involved in the anchoring of the AChRs in the synaptic membrane, have an abnormal pattern of AChR distribution, a reduced level of AChRs, and a lower stability of receptors in the postsynaptic membrane (Grady et al., 2000, 2003). Rescue of the synaptic phenotype in α-$db^{-/-}$ muscle fibers required expression of phosphorylatable wild-type α-dystrobrevin1 (α-DB1),

N. Schmidt, M. Akaaboune, and N. Gajendran contributed equally to this paper.

Correspondence to Mohammed Akaaboune: makaabou@umich.edu; or Hans Rudolf Brenner: Hans-Rudolf.Brenner@unibas.ch

Abbreviations used in this paper: AChE, acetylcholine esterase; AChR, acetylcholine receptor; α-BTX, alpha-bungarotoxin; α-DB, alpha-dystrobrevin; NMJ, neuromuscular junction; NRG, neuregulin.

The Rockefeller University Press $30.00
J. Cell Biol. Vol. 195 No. 7 1171–1184
www.jcb.org/cgi/doi/10.1083/jcb.201107083

which serves as a substrate for tyrosine kinases (Grady et al., 2003). However, the signaling pathway inducing phosphorylation of α-DB1 remains unknown.

Here we demonstrate a new role of NRG1/ErbB signaling in the maintenance of the NMJ postsynaptic membrane. In particular, we found that NRG1/ErbB signaling is critical for the stability of the AChRs, selectively of recycled AChRs, in the synaptic membrane and for the structural integrity of the postsynaptic apparatus. Structural changes in the postsynaptic apparatus of *erbb2/4*$^{-/-}$ synapses are coupled to reduced effectiveness of neuromuscular impulse transmission. Finally, we demonstrate that α-DB1 is a substrate for ErbB receptor tyrosine kinases, and that dephosphorylation of α-DB1 by ErbB deletion loosens AChRs in agrin-induced AChR clusters. Our experiments combined therefore indicate that NRG/ErbB, by phosphorylation of α-DB1, stabilizes the postsynaptic apparatus and, thus, contributes to anchoring the AChRs in the synaptic membrane.

Results

Deletion of NRG/ErbB accelerates the removal of AChRs from NMJs in vivo

In our previous work we showed that neuromuscular NRG/ErbB signaling is not necessary for synapse-specific expression of genes by subsynaptic nuclei of the mouse NMJ (Fig. S1; Escher et al., 2005).

To examine whether ErbB-mediated signaling is, instead, involved in regulating the stability of postsynaptic AChRs at the NMJ, the sternomastoid muscle of wild-type and *erbb2/4*$^{-/-}$ mice (Escher et al., 2005) was labeled to saturation in vivo with fluorescent α-bungarotoxin (α-BTX)–Alexa 594, and the decline in fluorescence of labeled AChRs was monitored over time. In *erbb2/4*$^{-/-}$ NMJs the residual fluorescence normalized to that at the time of labeling was significantly lower than in wild-type synapses (Fig. 1 a; ∼30% vs. 60% at 72 h). This indicates that the lack of ErbB-mediated signaling increases the rate of synaptic AChR removal.

A significant fraction of internalized AChRs recycle back into the postsynaptic membrane and intermingle with preexisting (i.e., not yet internalized) AChRs (Bruneau et al., 2005a; Bruneau and Akaaboune, 2006). We next examined if these two receptor pools are differentially affected by the loss of NRG/ErbB signaling. Therefore, the different AChR pools were fluorescently labeled as described in the Materials and methods section. Doubly labeled synapses (preexisting and recycled AChRs) on the surface of the muscle were immediately imaged and then reimaged 24, 48, and 72 h later. To exclude an effect of AChR labeling on electrical muscle activity and, thus, on AChR cycling, muscles were labeled with a low dose of α-BTX–biotin, leaving impulse transmission largely normal (Akaaboune et al., 1999). We found that fluorescence of recycled receptors in *erbb2/4*$^{-/-}$ muscles was lost more rapidly than in wild-type muscles (Fig. 1 b). In contrast, the loss of preexisting receptors in *erbb2/4*$^{-/-}$ muscles was nearly the same as that at wild-type synapses (Fig. 1 b). These results show that NRG/ErbB signaling is involved in controlling the stability of recycled, but not of nonrecycled AChRs in the postsynaptic muscle.

Genetic and pharmacological abolishment of ErbBs accelerates the migration of recycled receptors to the perisynaptic membrane

AChRs move between junctional and perijunctional regions (Akaaboune et al., 1999, 2002), and receptors lost from the synaptic to the perisynaptic membrane condense into small accumulations (called AChR puncta below) that are thought to be internalized (Akaaboune et al., 1999). Having shown that the lack of NRG/ErbB signaling promotes selectively the removal of recycled AChRs (Fig. 1 b) from the synapse, we next examined whether the migration of synaptic AChRs to the perisynaptic membrane and/or their internalization were altered in mutant mice. By comparing AChR puncta doubly stained with α-BTX–Alexa 594 and with Mab35 in unpermeabilized muscle, changes in the rates of internalization of AChR puncta versus changes in AChR migration can be resolved (Fig. S2). Using this approach, we thus compared the number of puncta containing preexisting and recycled AChRs in the perisynaptic surface membrane of *erbb2/4*$^{-/-}$ and wild-type muscles. Receptors were stained as indicated in Materials and methods, and 2 d later, surface receptors were immunostained with (Mab35)/Alexa 488 (Fig. 2 a).

Counts of the number of puncta in the perisynaptic membrane containing red (recycled) and blue (preexisting) AChRs showed that the number of puncta containing preexisting AChRs was no different in mutant and in wild-type synapses (Fig. 2 b). In contrast, the number of puncta containing recycled AChRs in *erbb2/4*$^{-/-}$ muscle was about twice that in wild-type muscle (Fig. 2 b). This is consistent with the increased loss of recycled AChRs from the synaptic membrane (Fig. 1 b). Co-staining surface AChRs with anti-AChR antibody (green) showed that for recycled AChRs, the number of both surface and internalized AChR puncta in mutant mice was about twice that in the wild-type mice (Fig. 2 b). Thus, although there were twice as many puncta in the perijunctional zone of mutant mice, the fraction of those puncta that were internalized was essentially the same as in the wild-type mice (2.00 vs. 2.2). This indicates that NRG/ErbB signaling controls the migration of AChRs from synaptic to perisynaptic sites; in contrast, their internalization from the perisynaptic zone is not affected.

With *erbb2*$^{-/-}$ synapses (Leu et al., 2003) showing similar declines in synaptic AChR densities and miniature endplate current amplitudes as *erbb2/4*$^{-/-}$ synapses (Escher et al., 2005), we examined *erbb2*$^{-/-}$ synapses for increases in AChR puncta and in perisynaptic AChR streaks, another characteristic of *erbb2/4*$^{-/-}$ NMJs. Indeed, both of these characteristics as well as the incidence of perforations in synaptic AChR clusters were increased (see following paragraph), suggesting that the synaptic changes observed were primarily, if not entirely, due to *erbb2* deletion (unpublished data).

Finally, as in *erbb2/4*$^{-/-}$ muscles, both the development of streaks of AChRs as well as enhanced migration of AChRs to the perisynaptic membrane was also seen in wild-type muscles that had been treated for 8 h with tyrphostins AG1478 and AG879 (10 μM), which are blockers of ErbB4 and ErbB2, respectively (Fig. S3; Fukazawa et al., 2003; Woo et al., 2007).

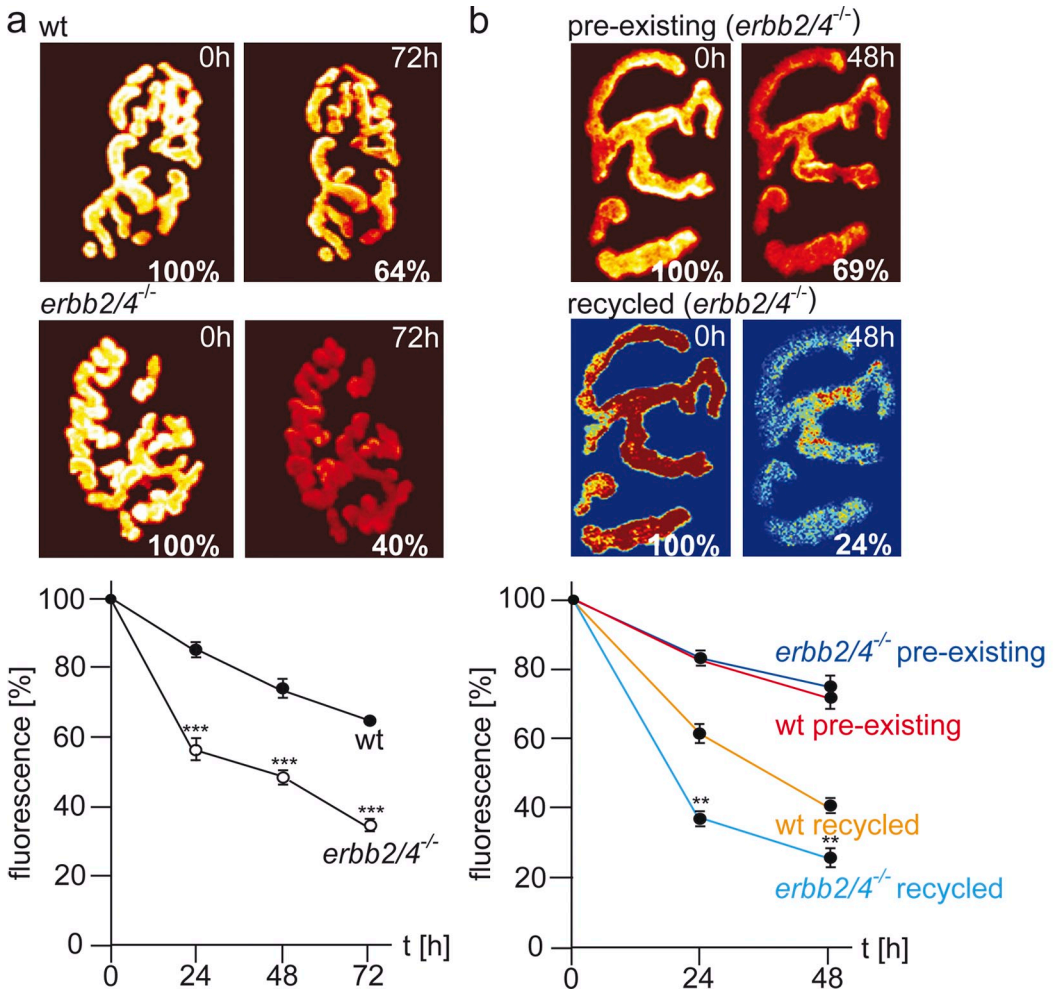

Figure 1. **Deletion of NRG/ErbB signaling increases removal of recycled receptor from the postsynaptic membrane.** (a) The sternomastoid muscle of *erbb2/4*$^{-/-}$ and wild-type mice was labeled with a saturating dose of α-BTX–Alexa 594, and superficial synapses were immediately imaged at time 0 and reimaged 1, 2, and 3 d later. The total fluorescence intensity of each AChR cluster was normalized to 100% at initial imaging. Examples of NMJs shown in pseudocolor provide a linear representation of the density of AChRs at the times indicated (top). Graph summarizing the removal of AChRs in wild-type and *erbb2/4*$^{-/-}$ synapses over the indicated time (mean percentage of fluorescence intensity ± SEM; *n* = 14–30 synapses from 3 animals [2 for *erbb2/4*$^{-/-}$ at 24 h] for each data point). Note that AChRs are removed significantly faster from *erbb2/4*$^{-/-}$ than from wild-type synapses. (b) Recycled and nonrecycled (preexisting) AChRs were fluorescently labeled with nonblocking doses of α-BTX–biotin (see Materials and methods). Doubly labeled synapses were imaged immediately and reimaged 24 and 48 h later. Data give mean percentage (±SEM) of residual fluorescence intensity relative to that at t = 0. Graph summarizing the results obtained from 4–18 synapses from three animals for each data point (bottom). The removal of recycled but not of preexisting AChRs is selectively increased in *erbb2/4*$^{-/-}$ mutant synapses.

The similarity of effects upon pharmacological and genetic ErbB deletions suggests that the tyrphostins used acted by blockade of ErbBs.

Lack of ErbB receptors causes structural damage to NMJs

High resolution confocal microscopy revealed that mutant mice often have small areas within the synaptic AChR cluster that are devoid of receptors, giving the cluster a perforated appearance (Fig. 3 b). About 45% of mutant synapses showed AChR cluster perforations between 17–21 d after birth, which is higher than in wild-type muscles (~10%). The incidence of formation of holes increased with age. By 1 yr nearly 100% of mutant synapses had at least one AChR hole, whereas less than 60% of control synapses were affected (Fig. 3 c). These results indicate that loss of NRG/ErbB signaling accelerates postsynaptic fragmentation.

To see whether AChR holes developed from focal receptor loss from the synaptic cluster, we double labeled adult synapses (2 mo) for AChRs (α-BTX–Alexa 488) and acetylcholine esterase (AChE), using the snake toxin fasciculin2 coupled to Alexa 594 (Peng et al., 1999; Krejci et al., 2006; Martinez-Pena y Valenzuela and Akaaboune, 2007). Fasciculin2 fluorescence was present at the sites from which AChR fluorescence was missing. In addition, we observed that entire branches of the NMJ were eliminated in mutant muscle (Fig. 3, d and e).

To examine whether the local loss of AChRs might result from local withdrawal of the nerve terminal, we labeled *erbb2/4*$^{-/-}$ synapses with antibodies to the presynaptic markers neurofilament and synaptophysin and with α-BTX–Alexa 594 to stain AChRs. Receptor holes were covered by presynaptic terminal branches (Fig. 3 f), suggesting that receptor holes are

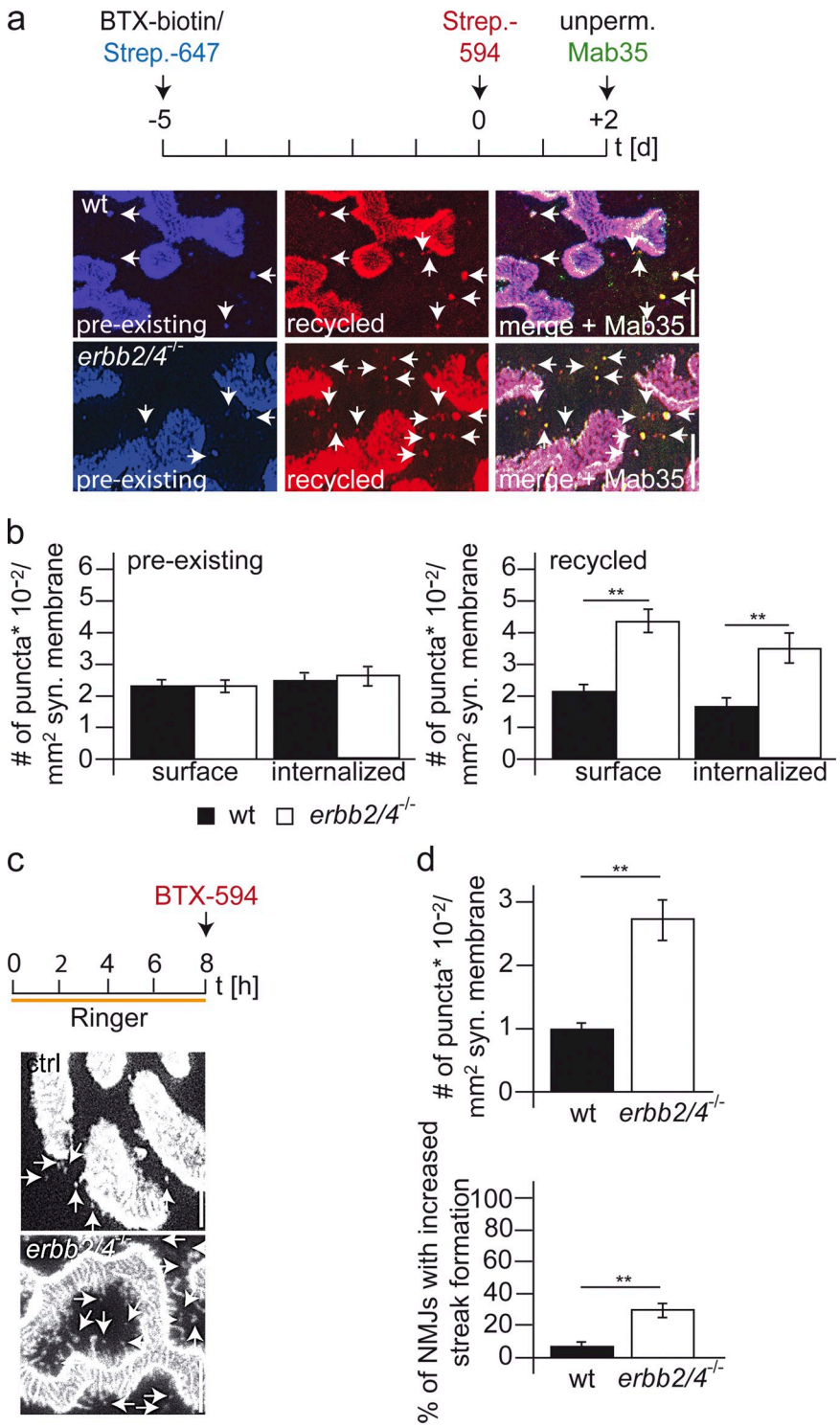

Figure 2. **Deletion of NRG/ErbB signaling increases AChR puncta containing recycled but not preexisting AChRs in the perisynaptic membrane.** (a) Labeling method for assessing the accumulation of AChRs in the perisynaptic membrane. 2 d after labeling recycled receptor, surface receptors were immunostained with the anti-AChR antibody Mab35 and Alexa 488 without permeabilization. Given are examples of high resolution confocal images of wild-type and *erbb2/4*$^{-/-}$ NMJs. Arrows mark puncta containing preexisting receptors (blue) and/or recycled (red) receptors localized in the perisynaptic membrane as suggested by costaining with nonpermeabilized AChR antibody Mab35 (green). Note the higher (twofold) accumulation of surface puncta containing recycled but not preexisting AChRs in *erbb2/4*$^{-/-}$ NMJs than in the wild type. Bars, 5 µm. (b) Graphs summarizing the quantification of fluorescent data as illustrated in panel a. Surface and internalized AChR puncta are increased by similar proportions in *erbb2/4*-deficient (2.00 ± 0.26-fold for surface and 2.2 ± 0.37-fold for internalized puncta; *n* = 29–30 synapses from three mutant and three wild-type animals) relative to wild-type muscle, indicating unchanged internalization rates. Therefore, the loss of NRG/ErbB signaling accelerates specifically the migration of recycled AChRs from the synaptic sites. (c and d) Endplates in *erbb2/4*$^{-/-}$ muscle acutely stained with α-BTX–Alexa 594 show increased numbers of perisynaptic AChR puncta (32 NMJs from three wild-type and 25 NMJs from three *erbb2/4*$^{-/-}$ mice; **, P < 0.01) and formation of AChR streaks extending from synaptic into perisynaptic membrane (244 NMJs from three wild-type and 259 NMJs from three *erbb2/4*$^{-/-}$ mice; **, P < 0.01). Bars, 5 µm.

not due to localized withdrawal of the nerve due to a presynaptic defect resulting from the lack of ErbB-dependent back-signaling onto the motor neurons (Bao et al., 2003). Thus, the modified distribution of AChRs is a direct consequence of the loss of NRG/ErbB signaling to the subsynaptic membrane.

AChRs are an integral part of the synaptic scaffold to which they are anchored. Thus, the focal loss of AChRs from the synaptic membrane may locally destabilize the postsynaptic apparatus (Bruneau et al., 2008). We therefore examined whether other components of the postsynaptic apparatus were lost from sites from which AChRs had disappeared. Indeed, immunoreactivity against MuSK, utrophin, and β-actin (Fig. 4 a), as well as rapsyn, sodium channel (NaCh), and β-dystroglycan (not depicted), was missing from sites where AChRs had disappeared. This result indicates that ErbB receptors are important not only for AChR stability, but also for the maintenance of postsynaptic scaffold proteins.

Additionally, we found that both rapsyn and utrophin were colocalized with increased number of perisynaptic AChR

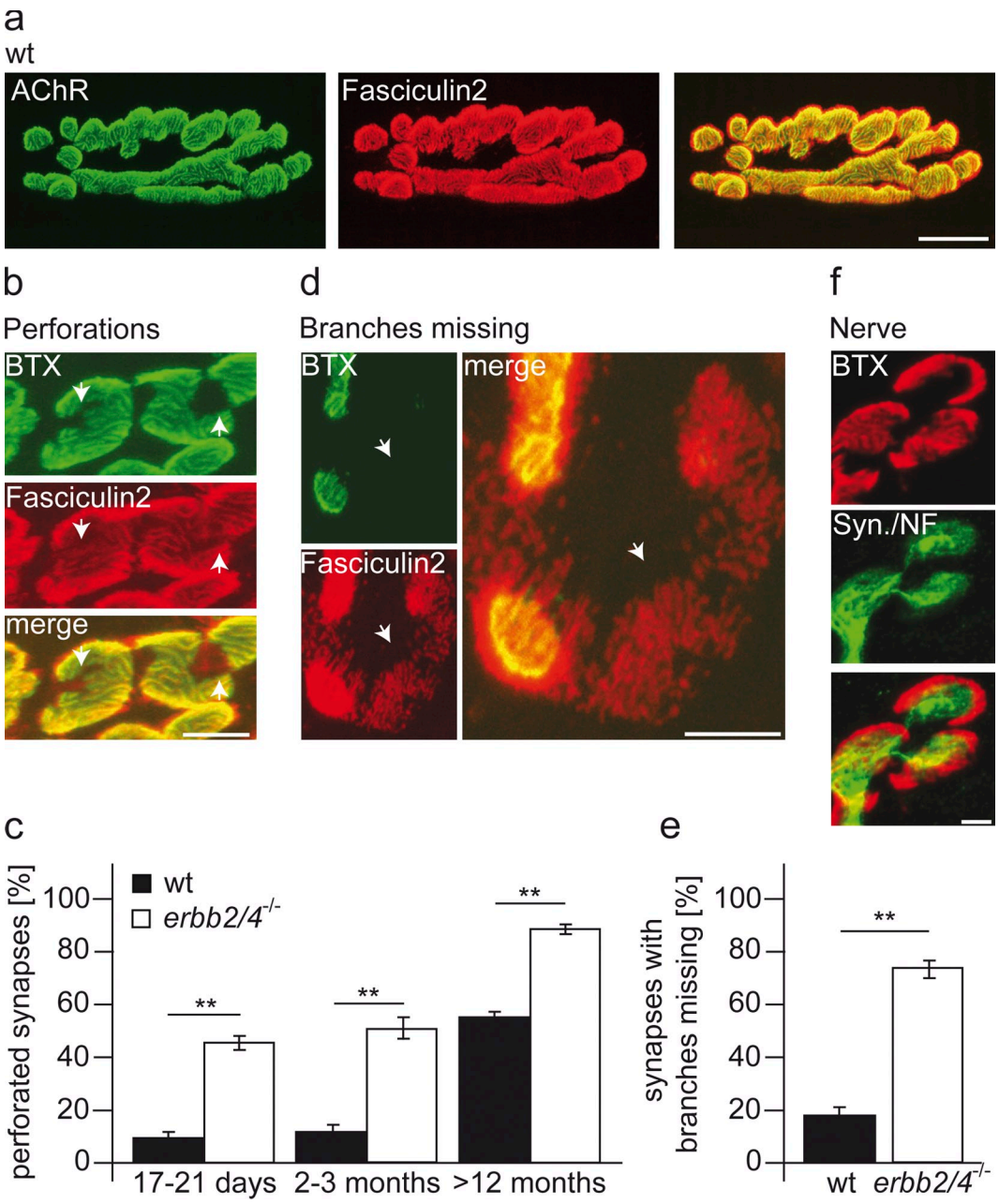

Figure 3. **Structural changes in *erbb2/4*$^{-/-}$ NMJs.** Synaptic AChR clusters develop perforations, and synaptic branches are lost. (a and b) Confocal images of adult wild-type (top) and *erbb2/4*$^{-/-}$ NMJs (a, center; b, center left) doubly labeled with fasciculin2–Alexa 594 (for AChE, red) and α-BTX–Alexa 488 (AChRs, green). Bars: (a) 10 μm; (b) 5 μm. Overlap of green and red is complete in wild-type but not in *erbb2/4*$^{-/-}$ NMJs, where AChE staining is observed where AChRs are missing (perforations). This indicates that perforations form in cluster regions previously occupied by AChRs. (c) Graph illustrating increased percentage of synapses with perforated clusters in 17–21-d, 2-mo-, and >12-mo-old *erbb2/4*$^{-/-}$ muscles compared with wild-type muscles of the same age (n > 100 synapses from at least three wild-type and three mutant mice for each age; **, $P < 0.01$). (d) High resolution images of a lost NMJ branch indicated by the presence of AChE staining without AChR staining. Micrograph from wild-type NMJ is given in panel a. Bar, 5 μm. (e) Graph summarizing the enhanced percentage of NMJs with missing branches in *erbb2/4*$^{-/-}$ muscle (n = 89 synapses from three mutant muscles and 63 synapses from three wild-type muscles at 2 mo; **, $P < 0.01$). (f) Presynaptic terminal branches remain at postsynaptic AChR cluster perforations, indicating that the latter are not due to focal withdrawal of the nerve terminal. AChRs (red) stained with α-BTX–Alexa 594, presynaptic terminal (green) stained with antibodies to synaptophysin and neurofilament. Bars, 5 μm.

puncta characteristic of mutant synapses (Fig. S4), mirroring the focal loss of the postsynaptic apparatus described above. These data suggest that the lack of NRG/ErbB signaling increases the loss of postsynaptic scaffold proteins from the synaptic sites to the perisynaptic region.

Finally, we examined the ultrastructure of the postsynaptic apparatus in NMJs of *erbB2/4*$^{-/-}$ mice, using electron microscopy. Although synaptic vesicles had a normal distribution in the presynaptic nerve terminals of both mutants and controls, the structure of the postsynaptic apparatus was abnormal in the mutants, with a scarcity of synaptic folds in the synaptic membrane (Fig. 4 b). Consistently, high resolution confocal microscopy of the AChR-rich interfold ridges suggested the scarcity of folds in mutant NMJs: Within an endplate a loss AChR-positive ridges

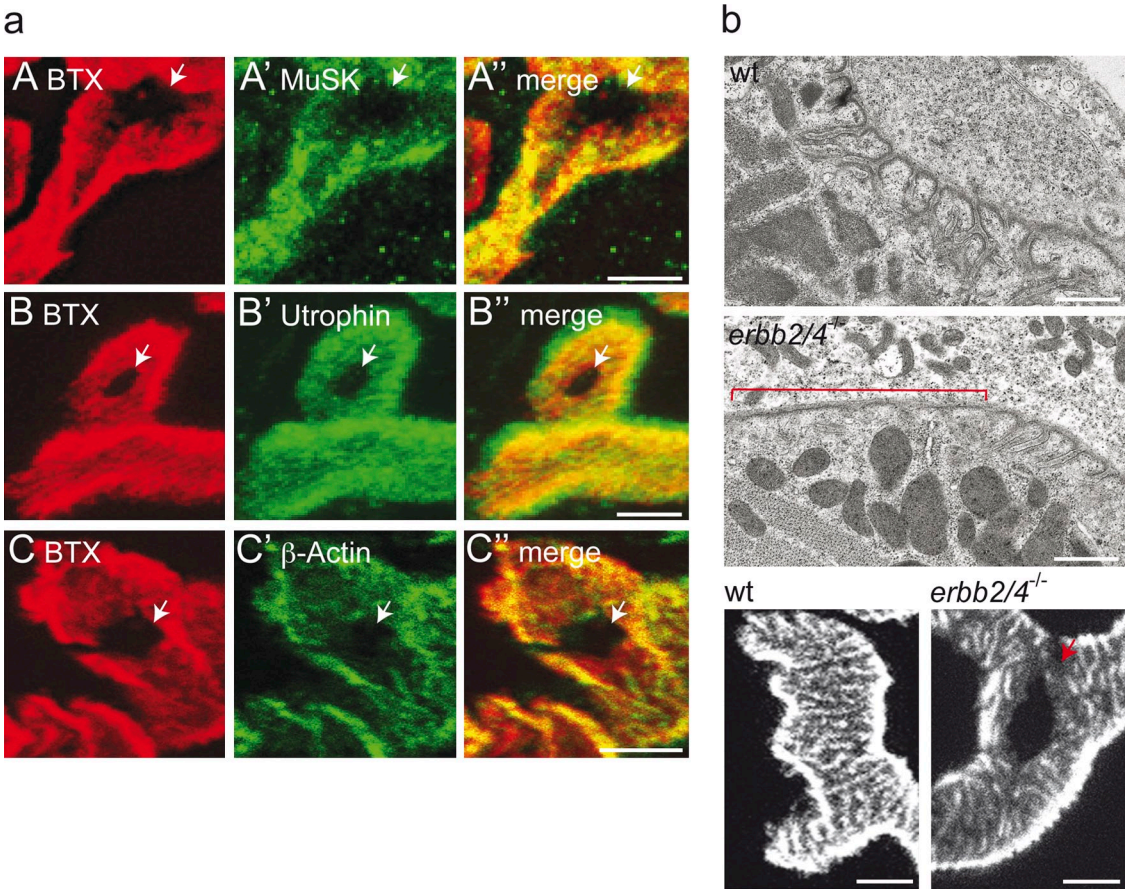

Figure 4. **MuSK and components of the subsynaptic apparatus are lost from AChR cluster perforations of *erbb2/4*$^{-/-}$ synapses.** Junctional folds are locally lost. (a) Sternomastoid muscle from 2-mo-old *erbb2/4*$^{-/-}$ mice were fixed and stained with α-BTX–Alexa 594 and antibodies to the indicated proteins. Note that all tested proteins are concentrated at synaptic sites except in perforations from where receptors have been lost. A′: MuSK, B′: utrophin, C′: β-actin. Bars, 5 µm. (b) Electron micrographs of control and *erbb2/4*$^{-/-}$ muscle (top and middle panel). Nerve terminal endings appeared normal in both mutant and wild type, but in the former synaptic folds were scarce or even lacking (bracket). The mean numbers of fold openings per synaptic contact length were 0.86 ± 0.1 (n = 19) in *erbb2/4*-deficient and 1.25 ± 0.07 (n = 18) in wild-type muscles. Bottom: high resolution confocal images of wild-type and *erbb*$^{-/-}$ NMJs labeled with α-BTX–Alexa 594. Note that the net loss of folded structure of the postsynaptic membrane primarily in the vicinity of cluster perforations (arrowhead).

did not evenly affect all subclusters, but was preferentially near areas of cluster perforations (Fig. 4 b). Together, these experiments suggest that ErbB deficiency structurally destabilizes the subsynaptic membrane.

Lack of ErbB receptors compromises impulse transmission

The abnormalities of ultrastructure and molecular organization described in the previous section in erbb2*/4*$^{-/-}$ muscle involve features of the NMJ that are known to affect the efficacy of neuromuscular transmission (Slater, 2008). To assess that efficacy, we compared isometric tetanic tension generated by mutant and wild-type soleus muscles in response to 50- and 120-Hz trains of stimuli to the soleus nerve. The tension in response to stimulating the nerve, relative to that in response to stimulating the muscle directly, was taken as a measure of the efficacy of neuromuscular impulse transmission (Witzemann et al., 1996).

In physiological Krebs solution, tensions to nerve and muscle stimulations were identical, both in *erbb2/4*$^{-/-}$ and in age-matched wild-type muscles (Fig. 5). To look more critically at the safety factor for neuromuscular transmission, we added d-tubocurarine (d-TC) to wild-type muscles to cause a partial block of AChRs. At a concentration of 340 nM there was a just-detectable reduction in the tetanic contraction in response to nerve, but not to muscle stimulation. When the same d-TC concentration (340 nM) was applied to *erbb2/4*$^{-/-}$ muscles (five mice), profound impairment of nerve-induced tetanic contractions in mutant muscles was induced (Fig. 5). These results indicate that *erbb* deletion lowers the safety factor of synaptic transmission.

ErbBs stabilize agrin-induced AChR clusters in cultured myotubes by phosphorylation of α-dystrobrevin1

Next, we examined a potential mechanism by which ErbB signaling might control the stability of the postsynaptic membrane. ErbB receptors have tyrosine kinase activity, and tyrosine phosphorylation is critical for synaptic plasticity. In mice deficient in α-dystrobrevin (α-DB), the phenotype of endplates (Banks et al., 2003) resembles in some aspect that in *erbb2/4*$^{-/-}$ mutants; conspicuously, the neuromuscular phenotype of *α-db*$^{-/-}$ muscle can only be rescued by exogenous α-DB1 containing

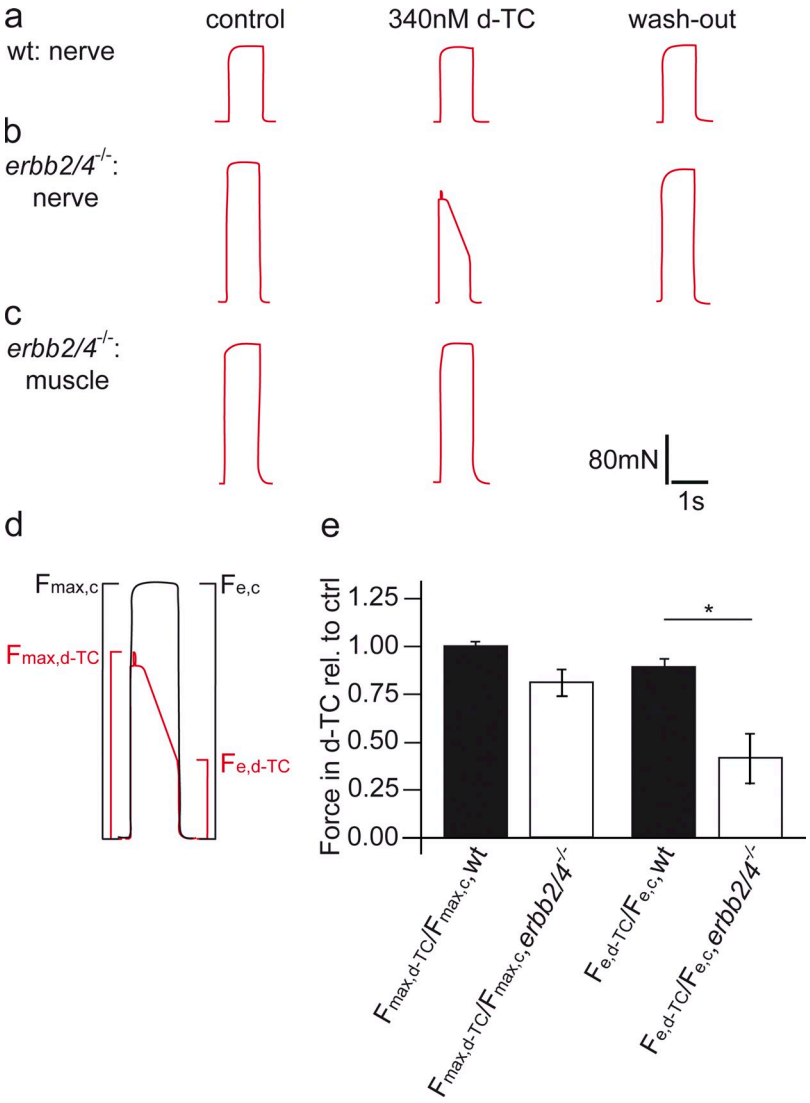

Figure 5. **Impulse transmission at synapses in *erbb2/4*$^{-/-}$ muscle is impaired.** (a) Isometric force of wild-type soleus muscle in response to a 120-Hz stimulus train to the soleus nerve. From left to right: in normal saline, in saline containing 340 nM d-tubocurarine-Cl (d-TC), after 30 min wash-out. (b) Isometric force of an *erbb2/4*$^{-/-}$ muscle (same protocol as in panel a). Note depression of contraction by 340 nM d-tubucurarine and complete recovery of contraction after wash-out. (c) Force developed by the same muscle as in b, but in response to muscle stimulation. Note that contraction is not affected by 340 nM d-tubocurarine-Cl. (d) Example of evaluation of tension recordings as illustrated in a and b. F_{max}, maximum isometric force developed during nerve stimulus train; F_e, isometric force at end of train; subscripts c, d-TC refer to forces developed in control and in d-TC–containing solutions, respectively. (e) Graph summarizing depression of responses in wild-type and *erbb*-deficient muscle treated with 340 nM d-TC analyzed as illustrated in d. Note the impairment of neuromuscular transmission during tetanic nerve stimulation in *erbb2/4*$^{-/-}$ muscles (n = 4 wild-type and 5 *erbb2/4*$^{-/-}$ muscles).

intact tyrosine phosphorylation sites (Grady et al., 2003). Therefore we sought to test whether NRG/ErbB signaling stabilizes agrin-induced AChR clusters in cultured myotubes via the phosphorylation of α-DB1.

If the stability of agrin-induced AChR clusters is NRG/ErbB-dependent in wild-type muscle and if this process is mediated by phosphorylation of α-DB1, the stability of AChRs should not be affected by the presence of NRG in *α-db*$^{-/-}$ myotubes. To test this prediction, cultures were first treated with a function-blocking antibody (Meier et al., 1998) to neutralize NRG1β activity secreted by the myotubes. Exogenous NRG1β was then added to test cultures (Fig. 6 a). Indeed, in wild-type myotubes NRG1β neutralization reduced the size of agrin-induced AChR clusters compared with myotubes exposed to NRG1β; in contrast, AChR clusters in *α-db*$^{-/-}$ myotubes (which have reduced AChR cluster size; Pawlikowski and Maimone, 2009) were not affected by NRG1 neutralization or addition (Fig. 6 b). However, NRG dependence of AChR cluster stability could be rescued when a wild-type, i.e., phosphorylatable, but not when a mutant, i.e., nonphosphorylatable, construct of α-DB1 (Grady et al., 2003) was expressed in *α-db*$^{-/-}$ myotubes (Fig. 6 c). Note that in cultures that were not treated with neutralizing antibody, AChR cluster size was not affected by the addition of exogenous NRG1β (not depicted), indicating that secreted NRG1β activity was sufficient to fully saturate AChR stability (see also Fig. 7). These data demonstrate on the functional level that NRG/ErbB stabilizes agrin-induced AChR clusters via a process involving phosphorylation of α-DB1.

To test whether NRG/ErbB phosphorylates tyrosine residues in α-DB1, C2C12 and primary wild-type myotubes were cultured on a substrate of agrin-impregnated laminin (Lacazette et al., 2003) to induce large areas of subsynaptic apparatus. Given that both pharmacological and genetic abolishment of ErbB function enhance AChR migration at endplates in vivo (Fig. 2 and Fig. S3), cultured myotubes (C2C12 and primary wild type) were incubated with 5 µM ErbB blockers or 5 nM NRG1β either in the presence or absence of peroxivanadate (inhibitor of phosphatases), and the phosphorylation of α-DB1 was analyzed. As α-DB1 is complexed with utrophin and syntrophin, lysates were immunoprecipitated with an antibody (SYN1351) recognizing α- and β-syntrophins (Froehner et al., 1987). Precipitates were denatured and blotted with

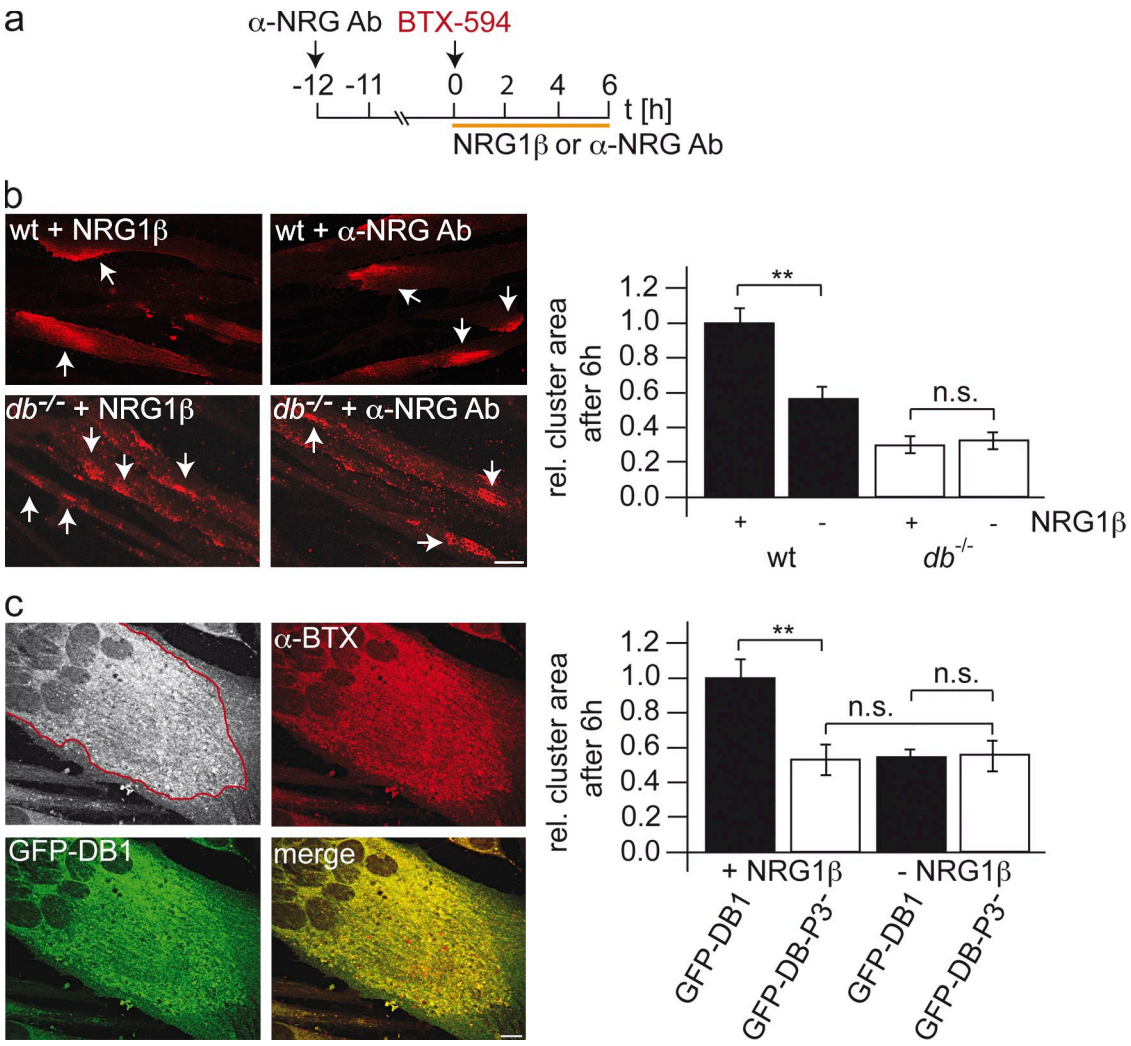

Figure 6. **The stability of agrin-induced AChR clusters in cultured myotubes depends on the presence of NRG and on phosphorylation of α-dystrobrevin1.** Myoblasts were seeded on laminin substrates containing focal agrin deposited by agrin-transfected COS-1 cells, and differentiated. AChR clusters were induced where myotubes contacted agrin deposits. (a) Experimental protocol. Myotubes (wild type, transfected wild type, or α-$db^{-/-}$ mutant) were preincubated for 12 h in the presence of 30 µg/ml anti-NRG1β antibody to neutralize autocrine NRG activity and then stained with α-BTX–Alexa 594 (red). In one set (labeled +NRG1β), antibody was then removed and replaced by 5 nM NRG1β; in the other set (labeled −NRG1β), removed antibody was replaced with a fresh dose of antibody. Both sets of cultures were fixed after 6 h. (b) NRG1β stabilizes AChR clusters only in wild-type, but not in α-$db^{-/-}$ mutant myotubes. Left: Examples of agrin-induced AChR clusters (marked by arrows) in wild-type and α-$db^{-/-}$ mutant myotubes maintained in the presence and absence of NRG1β, respectively. Both sets of cultures were fixed after 6 h. Bar, 20 µm. Right: Quantification of AChR cluster area (n = 64–86 clusters analyzed per group; data from three parallel cultures). (c) NRG1β stabilizes agrin-induced AChR clusters in α-$db^{-/-}$ myotubes only when expressing wild-type α-DB1, but not when expressing nonphosphorylatable α-DB1. Agrin-induced AChR clusters in α-$db^{-/-}$ mutant myotubes transfected to express GFP-tagged wild type (GFP-α-DB1) or nonphosphorylatable (GFP-α-DB1-P3-) α-dystrobrevin1 (Grady et al., 2003) are compared. Left: Confocal images shows "rescued" agrin-induced AChR cluster (red) in GFP-DB1–expressing myotubes (green). Elevated GFP-DB1 was colocalized with AChR clusters. Bar, 5 µm. Right: Quantification of AChR cluster area (n = 30–40 clusters analyzed per group). Note the inability of exogenous NRG1β to stabilize AChR clusters in the absence of phosphorylatable α-dystrobrevin1.

anti-phosphotyrosine (4G10), anti–α-DB1, and anti–α-syntrophin antibodies (Adams et al., 2000).

Fig. 7 a shows that there was substantial phosphorylation of α-DB1 in untreated cells, and added NRG1β did not further increase phosphorylated α-DB1 beyond this basal level, presumably due to autocrine ErbB activation (Meier et al., 1998) and consistent with full AChR stabilization by secreted NRG1β in the absence of neutralizing antibody (see Fig. 6 b and text above). In contrast, pharmacological blockade of NRG/ErbB signaling substantially reduced phosphorylation of α-DB1 both in primary and C2C12 myotubes. Similar results were obtained when myotubes were incubated with 5 µM ErbB2 blocker alone (Fig. S5). In C2C12 myotubes, α-DB1 phosphorylation and its blockade by ErbB inhibitors could also be resolved without peroxivanadate pretreatment. However, the level of tyrosine-phosphorylated α-DB1 was then substantially lower (Fig. 7 a, legend), indicating that inhibition of dephosphorylation allows accumulation of phosphorylation.

Abolishment of α-DB1 phosphorylation by ErbB blockers was also observed when α-DB1 was pulled down directly from C2C12 myotubes (Fig. 7 b). In contrast, α-syntrophin phosphorylation was not affected by ErbB blockade, at least on the time scale investigated (Fig. 7 a). Moreover, the abundance of neither α-syntrophin nor utrophin in the precipitate

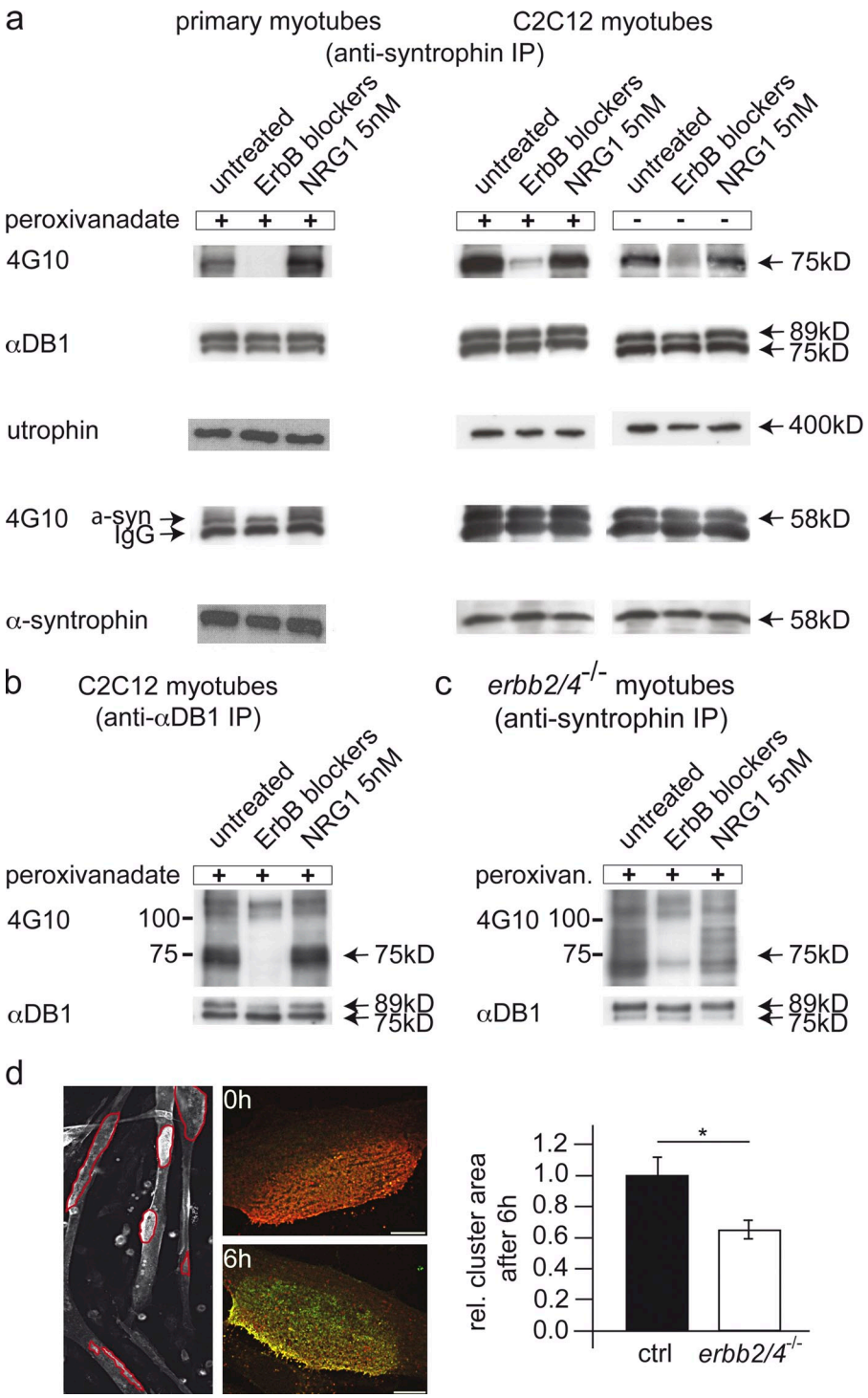

Figure 7. **Blockade of NRG/ErbB signaling abolishes phosphorylation of *α-dystrobrevin1* and destabilizes agrin-induced AChR clusters.** (a) ErbB blockers AG879 and AG1478 (5 μM each) abolish phosphorylation of α-DB1. α-DB1 was pulled down with an anti-syntrophin antibody from myotubes grown on laminin coated with neural agrin. After blotting, tyrosine phosphorylation was detected with the anti-PY antibody (4G10) and precipitated proteins with the respective antibodies. Syntrophin blots served as loading controls. Phosphorylation of α-DB1 in absence of exogenous NRG1 was due to autocrine action of NRG1β secreted from the myotubes (Jones et al., 1999), preventing further phosphorylation by exogenous NRG1β. For vanadate-pretreated samples in the 4G10 blots the exposure after ECL development was ~10 times shorter than for nontreated samples, reflecting a very rapid dephosphorylation process. (b) Same experiment as in panel a, except that IP was with the anti–α-DB1 antibody used in panel a for protein detection. Phosphorylation of the 75-kD isoform of α-DB1, but not of other proteins pulled down by anti–α-DB1 antibody, is blocked by pharmacological ErbB blockade. Note that the 75-kD band, when detected with α-DB1 antibody, appears stronger in intensity, as the immunoprecipitation with the α-DB1 antibody pulls down not only the α-DB1 associated with the syntrophin–DG complex (as observed using anti-syntrophin 1351 antibodies) but also uncomplexed α-DB1. The positions of size markers are indicated. (c) Genetic deletion of ErbBs abolishes phosphorylation of α-DB1 by NRG1β. Same experiment as in panel a, except that *erbb2/4*$^{-/-}$ myotubes were used, and a larger section of the blot is shown. No bands can be resolved at 75 kD in blots from ErbB-deficient cells, unlike in the α-DB1 pull-downs of C2C12 myotubes performed under similar conditions (b). The clear band just below 75 kD cannot be α-DB1 because it is not observed in IPs with the anti–α-DB1 antibody. The positions of size markers are indicated. (d) Genetic abolishment of ErbBs reduces the stability of agrin-induced AChR clusters. Left: Example of agrin-induced AChR clusters and manual delineation of their edges for estimation of cluster area after staining with α-BTX–Alexa 594. Agrin was deposited on laminin substrate as described in Materials and methods. Confocal image of cluster post-stained at 0 h with α-BTX–Alexa 488 shows only original (red) staining. 6 h later, original receptors (red) prevail at center and newly inserted (green) AChRs at cluster periphery. Bars, 10 μm. Right: Quantification of area occupied by original AChRs stained at 0 h and those remaining at 6 h. Note that the decrease in cluster size is more rapid in *erbb2/4*$^{-/-}$ than in wild-type myotubes (n = 60–77 clusters analyzed). The positions of size markers (in kD) are indicated.

was affected, demonstrating that the stability of the complex by itself is independent of the phosphorylation/dephosphorylation mechanism.

To exclude the possibility that phosphorylation of α-DB1 was due to ErbB1 signaling, we used the ErbB2 blocker AG879 alone (5 μM, which at this concentration does not block EGFR signaling; Levitzki and Gazit, 1995) and found that it blocked α-DB1 phosphorylation (Fig. S5). Based on this result, i.e., that phosphorylation of α-DB1 was not due to EGFR signaling, we used both ErbB4 and ErbB2 blockers to completely eliminate all NRG1 signaling, i.e., also that through ErbB4. Second, we assayed phosphorylation of α-DB1 in α-syntrophin pull-downs from myotubes derived from immortalized *erbb2/4*$^{-/-}$ myoblasts. Consistent with the data described above, phosphorylation

of α-DB1 could not be detected, either in the absence or the presence of exogenous NRG1β (Fig. 7 c). The result was similar in pull-downs with anti-αDB1 antibody. Thus, abolishment of α-DB1 phosphorylation was due to ErbB blockade rather than to a nonspecific effect of the pharmacological ErbB blockers (Fig. 7 c). These experiments combined show that NRG/ErbB signaling can phosphorylate α-DB1. Interestingly, the amount of the 75-kD α-DB1 isoform was reduced in the DGC compared with the 89-kD isoform in *erb2/4*$^{-/-}$ myotubes. Whether this reduction is due to the prolonged absence of NRG signaling is not clear, but these results demonstrate clearly that the absence of NRG signaling through ErbB2/4 results in a dramatic reduction of phosphorylated α-DB1 in the dystrophin–utrophin glycoprotein complex (DGC).

Unlike in cultured myotubes, phosphorylation of α-DB1 could not be detected when assayed in synaptic and in extrasynaptic fragments of diaphragm from *erbb2/4*$^{-/-}$ and wild-type mice, respectively (not depicted). Possible explanations are that synaptic α-DB1 was occluded by nonsynaptic α-DB1 and that muscles did not tolerate pretreatment with phosphatase inhibitor; indeed, α-DB1 phosphorylation could so far be resolved in cultured myotubes only after treatment with phosphatase inhibitors (Nawrotzki et al., 1998; Grady et al., 2003), so the equivalent experiment could not be performed.

Next, we examined whether genetic deletion of ErbBs in myotubes is associated with impaired stability of AChR clusters, as it is at *erbb2/4*$^{-/-}$ endplates in vivo (Figs. 1 and 3). To this end, myotubes derived from *erbb2/4*$^{-/-}$ and from wild-type neonatal muscles were grown on laminin substrates focally impregnated with neural agrin (Jones et al., 1996). Clusters were stained with α-BTX–Alexa 594 and cells were incubated for 6 h at 37°C to allow turnover of labeled receptors. As shown in Fig. 7 d, the area of AChR clusters decreased more rapidly with time in *erbb2/4*$^{-/-}$ than in wild-type myotubes. This result indicates acceleration of AChR migration out of the cluster in *erbb2/4*$^{-/-}$ myotubes; as a consequence, cluster size appeared reduced more rapidly over time. Post-staining clusters with α-BTX–Alexa 488 after 6 h of culturing showed new AChRs (labeled green) prevailing at the cluster periphery, demonstrating that overall cluster size, i.e., including newly inserted AChRs, was maintained (Fig. 7 d). Resolving a differential effect on recycling AChRs was not possible because, unlike at mature NMJs, AChRs in myotubes do not recycle into clusters (Bruneau et al., 2005b). These data combined with those in Fig. 6 show that abolishment of NRG/ErbB signaling by removal either of NRG1β or of its receptors impaired receptor stability in agrin-induced AChR clusters.

Finally, we examined whether defective laminin expression at *erbb2/4*$^{-/-}$ synapses could account for the synaptic phenotype in the *erbb* mutant mice (Grady et al., 2000; Sunderland et al., 2000; Patton et al., 2001; Fukazawa et al., 2003). Immunocytochemical staining for laminin α5, β2, and γ1 showed no difference to wild-type synapses, however (not depicted). Together, these data indicate that both pharmacological and genetic ablation of NRG/ErbB signaling results in a lack of phosphorylation of α-DB1, and as a consequence destabilizes AChRs in agrin-induced AChR clusters.

Discussion

The present experiments show, by deletion of ErbB2 and ErbB4 receptors, that NRG1/ErbB signaling is essential for the maintenance of a normal number of AChRs at the adult NMJ, in agreement with a previous report in which NRG/ErbB signaling was impaired by deletion of one of the *nrg-1* alleles (Sandrock et al., 1997). However, synaptic phenotypes in these mutants cannot be compared at the quantitative level because in the former, neuromuscular NRG1/ErbB signaling was not completely abolished, and as indirect effects, e.g., via Schwann cells, cannot be excluded.

The present experiments now show that one mechanism by which NRG maintains synaptic AChR numbers is by enhancing the stability of their anchoring to the synaptic muscle membrane via activation of ErbBs and tyrosine phosphorylation of α-DB1. This is suggested by (i) the destabilization of AChRs observed upon pharmacological or genetic abolishment of ErbB receptor function at agrin-induced AChR clusters in myotubes as well as at adult NMJs in vivo; (ii) the dephosphorylation of α-DB1 in cultured myotubes; and (iii) the dependence of NRG-induced AChR cluster stabilization on the presence of α-DB, specifically of phosphorylatable α-DB1. These observations are consistent with previous studies showing that α-DB1 is a key component of the synaptic DGC that is essential for normal maturation and stabilization of the postsynaptic membrane by providing a molecular link between cytoplasmic F-actin and the basal lamina of the muscle fiber (Banks et al., 2003).

Consistent with our findings, the endplates in *erbb2/4*$^{-/-}$ muscles share some similarities with those observed in muscles lacking dystroglycan (Jacobson et al., 2001), α-syntrophin (Adams et al., 2000), utrophin (Deconinck et al., 1997b; Grady et al., 1997), and α-DB1 (Grady et al., 1999), which form the DGC. While common to both *erbb2/4*$^{-/-}$ and *α-db* mutant muscles are similar reductions in metabolic AChR half-life and in the number of synaptic folds, the reductions in AChR density and in the density of AChR streaks are both stronger in *α-db* mutants (Grady et al., 1997, 2000; Akaaboune et al., 2002; Escher et al., 2005). The synaptic phenotype in *erbb2/4*$^{-/-}$ mutant muscle would likely be milder than that in *α-db* mutant muscle because the lack of α-DB1 phosphorylation in *erbb2/4*$^{-/-}$ mutants may impair, but does not abolish, the formation of the syntrophin–dystrobrevin–utrophin complex; moreover, in *α-db*$^{-/-}$ mutants, not only α-DB1, but also α-DB2 isoforms are deleted, both of which contribute in part to the stability of the synaptic membrane in wild-type muscle, independently of whether they can be phosphorylated (Grady et al., 2003; Pawlikowski and Maimone, 2009). Nevertheless, the appearance of AChR holes at P17 (Fig. 3) as a consequence of the mere lack of phosphorylation of α-DB1 (as found here) would compare well with the late onset of the NMJ phenotype in *α-db*$^{-/-}$ mutants (Grady et al., 2000), where all α-DB isoforms are ablated.

NRG/ErbB-dependent phosphorylation/dephosphorylation of α-DB1 is a highly dynamic process. Specifically, 30 min preincubation with peroxivanadate was sufficient to increase the level of tyrosine-phosphorylated α-DB1 in myotubes substantially beyond that in untreated cells, a process that could be

prevented by 30 min of pharmacological ErbB blockade (Fig. 7). Similar concentrations of blockers increased AChR migration within hours (Fig. S3). Considering that overall anchoring of AChRs in the synaptic membrane is stable, it is remarkable that phosphorylation of α-DB1 and the resulting change in AChR stability are regulated by NRG/ErbB signaling on a time scale of minutes to hours.

How could the lack of NRG/ErbB signaling be linked to AChR instability? One possibility is that phosphorylation of α-DB1 may stabilize the DGC. Interestingly, the association of utrophin with syntrophin was not affected by ErbB blockade, at least in the pharmacologically blocked myotubes. This is unlike the ablation of α-syntrophin, which causes loss of utrophin and NOS from the synapse (Adams et al., 2000). Conspicuously, NRG/ErbB phosphorylated only the smaller of two α-DB1 variants precipitated either with anti-syntrophin or with anti–α-DB1 antibodies (Fig. 7).

How could abolishment of NRG/ErbB signaling affect specifically the migration of recycled, as opposed to nonrecycled (preexisting) AChRs and induce focal disappearance of AChRs and postsynaptic apparatus from the synaptic membrane? Even in wild-type muscle the removal of recycled is faster than that of nonrecycled AChRs (Bruneau et al., 2005a), suggesting that during the process of intracellular cycling, AChRs are modified/altered in a way to loosen/destabilize their interaction with the postsynaptic scaffold. The present data suggest that this interaction is further destabilized when α-DB1 is not phosphorylated. The resulting decrease in AChR density could then lead to the disintegration of the postsynaptic apparatus as we observed previously after focal dissipation of AChRs by laser illumination from clusters in cultured myotubes (Bruneau et al., 2008). The focal loss of AChRs may result from the uneven distribution of the AChRs over the entire synapse, with the rapid removal of recycled AChRs due to ErbB deficiency lowering AChR density locally to levels triggering local disassembly of the postsynaptic apparatus.

At the structural level, destabilization of the synaptic scaffold is suggested by the reduction in the number of folds in *erbb2/4*$^{-/-}$ mice. Defects in, or the absence of, a number of scaffold proteins including rapsyn, utrophin, dystrobrevin, dystroglycans are all associated with a similar reduction of the number of synaptic folds (Deconinck et al., 1997a,b; Grady et al., 1997, 1999, 2000). In line with this, the regions of the NMJs in *erbb2/4*$^{-/-}$ mice where folds are reduced appear preferentially where AChRs are lost. The proteins of the underlying scaffold are also reduced (Fig. 4) and appear with AChRs in perisynaptic puncta (Fig. S4). The focal loss of AChRs, the reduction of synaptic folds, and the loss of entire branches of subsynaptic AChR clusters may represent progressive stages of the same disassembly process of the synapse. The early formation of AChR cluster perforations in mutants (a process that in wild-type muscle was observed only at aged synapses) suggests that NRG/ErbB signaling at the NMJs might prevent the premature aging of synapses.

A high density of AChRs and voltage-gated sodium channels, and the presence of synaptic folds, are all important for the maintenance of a high safety factor for impulse transmission at the mammalian NMJ (Slater, 2008). Therefore, all the defects described above, in conjunction with a small overall reduction in AChR density (Escher et al., 2005), will impair the efficacy of synaptic impulse transmission. This is what we observe here (Fig. 5): The normal safety factor of neuromuscular transmission in rat soleus muscle is ∼3.5 (Wood and Slater, 1997). d-TC at 340 nM (as used here) lowers the amplitude of miniature endplate currents in wild-type mice by two thirds (Pennefather and Quastel, 1981), thus lowering the safety factor to ∼1.2. Based on these observations, the safety factor in the soleus of *erbb2/4*$^{-/-}$ mice was lowered by the d-TC treatment to critical levels where the functional effects of structural damage begin to affect impulse transmission during repetitive stimulation. The lowered safety factor may become detrimental when combined with its lowering as the animal ages (Valdez et al., 2010).

Numerous reports implicate NRG/ErbB signaling and components of the DGC in the development of normal brain function (Mei and Xiong, 2008; Waite et al., 2009). It is thus tempting to speculate that ErbB-dependent stabilization of receptors in synaptic membranes by phosphorylation of α-DB1 contributes to some of the processes involved in the functional maturation of the central nervous system.

Materials and methods

Animals

Erbb2/4$^{-/-}$ mice have been described previously (Escher et al., 2005). Unless noted otherwise, experiments were done on sternomastoid muscles from 8–12-wk-old mice. For surgery and in vivo staining, animals were anesthetized with ketamine (87 mg per kg body weight) and xylazine (13 mg per kg body weight). Postoperative analgesia was by four injections of buprenorphine at 12-h intervals. For acute experiments, tested agents were injected and bath applied to the sternomastoid muscle and replaced by freshly prepared agent solution every 60 min for 4 or 8 h. The viability of muscles exposed to drugs in vivo was ascertained from their contractions in response to nerve stimulation. Mice were sacrificed with CO_2. Animal handling was approved by the Cantonal Veterinary Office of Basel-Stadt.

Chemicals, antibodies, fusion constructs, and cell lines

ErbB inhibitors AG 879 and AG 1478 (EMD) were used at 10 µM (in vivo) or 5 µM (in culture), dynasore (Sigma-Aldrich) at 160 µM, and NRG-1β (R&D Systems) at 5 nM. AChRs were labeled with either α-BTX–Alexa594 (Invitrogen) or α-BTX-biotin followed by streptavidin–Alexa 488, 594 or 647 (10 µg/ml; Invitrogen) or anti-AChR antibody Mab35 (Developmental Studies Hybridoma Bank [DSHB], Iowa City, IA). Synaptic components were stained with antibodies against β-dystroglycan (DSHB), utrophin (DSHB), rapsyn (Thermo Fisher Scientific), β-actin (JLA20; DSHB), laminin α5 (a gift from L. Sorokin, University of Münster, Münster, Germany), laminin γ1 (Millipore), and laminin β2 (Santa Cruz Biotechnology, Inc.). The anti-MuSK and pan anti-Nav antibodies were kind gifts from M. Rüegg (University of Basel, Basel, Switzerland) and R. Levinson (University of Colorado, Denver, CO). Secondary antibodies conjugated to Alexa 488 were purchased from Invitrogen; Transferrin (Tf)-Alexa 647 or Tf-Alexa 488 from Sigma-Aldrich. Antibodies for biochemical experiments are listed in the respective paragraph below. Fusion constructs for GFP–α-DB1 and GFP–α-DB1-P3 were gifts from J.R. Sanes (Harvard University, Cambridge, MA) and C. Mouslim (University of Michigan, Ann Arbor, MI), respectively. *α-db*$^{-/-}$ myoblasts were kind gifts from B. Pawlikowski and M. Maimone (Upstate Medical University, State University of New York, Syracuse, NY).

In vitro measurements of muscle strength

Soleus muscles were dissected with the soleus/sciatic nerve attached and mounted in a muscle testing setup (Heidelberg Scientific Instruments). Before tension measurements began, muscles were left to equilibrate in Krebs Ringer's solution maintained at 30°C and gassed with 95% O_2/5% CO_2, and their resting length was adjusted to produce maximal twitch contraction

in response to single stimuli applied once every 2 min. Muscles were stimulated either indirectly via the sciatic nerve through a suction electrode, or directly via a pair of extracellular electrodes placed in the bath on both sides of the muscle. Muscle force was digitized at 4 kHz by using an AD Instruments converter and stimulated with 15-V pulses for 0.5 ms. Soleus tetanus was recorded in response to 1,100-ms pulses at 10–150 Hz (Delbono et al., 2007). After change of solutions, 30 min were allowed before tension measurements were resumed.

In vivo labeling, live animal imaging, and quantitative fluorescence measurements

To monitor AChR removal from the synapse, the sternomastoid muscle was labeled for 1 h with 5 µg/ml α-BTX–Alexa594 (a dose that has previously been demonstrated to be sufficient to saturate all receptors [Bruneau et al., 2005a]) and superficial synapses were imaged over 3 d.

To determine the removal rate of the different AChR pools (preexisting and recycled AChRs), the sternomastoid muscle of anesthetized mice was exposed to α-BTX-biotin (1 µg/ml, 10 min) followed by a single saturating dose of streptavidin–Alexa 488, so that synaptic transmission remained functional (Akaaboune et al., 2002). 5 d later, recycled receptors that had lost the streptavidin–Alexa 488 in the process of recycling (Bruneau et al., 2005a) and were reinserted into the synaptic membrane, were labeled with streptavidin–Alexa 594 . All controls for the specificity of the biotin–streptavidin dissociation have been worked out previously (Bruneau et al., 2005a). Doubly stained synapses (recycled [red] and preexisting [green] receptors) on the surface of the muscle were immediately imaged and reimaged 24 and 48 h later. The fluorescence intensity of labeled AChR at wild-type and *erbb2/4*$^{-/-}$ neuromuscular junctions was assayed using a quantitative fluorescence imaging technique, as described previously (Turney et al., 1996). This technique incorporates compensation for image variation that may be caused by spatial and temporal changes in the light source and camera between imaging sessions by calibrating the images with a nonfading reference standard. This technique involves repetitive imaging of the same fluorescent ligands. Thus, as long as we verified that labeling had reached saturation and that the image pixel intensity was not saturated, it was relatively trivial to get an accurate quantitative measurement of the relative number of AChRs. Image analysis was performed using a procedure written for Matlab (The Mathworks), which allows to approximate the background fluorescence by selecting a boundary region around the junction and subtracting it from the original image, and the mean and the total intensity was summed (Bruneau et al., 2005a; Martinez-Pena y Valenzuela et al., 2005). Total fluorescence intensity (a measure of the total number of AChRs) was expressed as 100% at the first view and normalized to this on each successive view.

To compare puncta number in *erbb2/4*$^{-/-}$ and control NMJs, preexisting AChRs were labeled with α-BTX-biotin (3 µg/ml, 90 min), followed by strepatavidin–Alexa 647 (10 µg/ml, 3 h). 5 d later, recycled AChRs were visualized by streptavidin–Alexa 594 (10 µg/ml, 3 h) and another 2 d later, surface AChRs were labeled by Mab35-antibody/Alexa 488 in nonpermeabilizing conditions. The number of fluorescent AChR puncta was determined in the vicinity of the NMJs. When puncta were counted in the perisynaptic region up to 100 µm on both sides of the synapse, we observed a significant drop in puncta number at 15–20 µm away from the synapse. Therefore, we reduced the area of interest to 25 µm from the synapse in favor of higher magnification, which did not affect the relative differences in puncta number in any of the conditions tested.

To study the effect of ErbB blockers and dynasore on the removal of AChR pools (recycled and preexisting AChRs), recycled AChRs of wild-type sternomastoid muscle were stained as described above and were then bathed immediately with both AG 879 and AG 1478 (10 µM), dynasore (160 µM), or Ringer's solution for 8 h. At the end of the experiment, surface AChRs were labeled with Mab35 without permeabilization. After fixation and mounting, superficial synapses were imaged confocally.

Immunocytochemistry

For immunostainings, muscles were fixed with PFA. Teased fiber bundles were blocked in PBS/20% normal goat serum (NGS)/ 1.5% Triton X-100 (1 h, 4°C) and stained with primary antibody in PBS/2% bovine serum albumin (BSA)/0.5% Triton X-100 (overnight, 4°C). In the case of extracellular epitopes, antibody was added directly. Extensive washing was followed by incubation of the fibers with α-BTX–Alexa 594 (1 µg/ml) and secondary antibody coupled to Alexa488 (45 min, room temperature).

Transferrin uptake was performed with Tf–Alexa 647 (15 µg/ml, 10 min, COS-1 cells on ice) or Tf–Alexa 488 (40 µg/ml, 45 min, sternomastoid muscle). After incubation in the absence or presence of dynasore (sternomastoid muscle: 160 µM for 4 h, COS-1 cells: dynasore previously used on muscle for 15 min) surface Tf was removed with ice-cold acetic acid/NaCl (0.2 M/0.5 M, 4 min). Muscles were stained with α-BTX–Alexa 594 (1 µg/ml, 1 h) and Tf-containing vesicles were quantitatively assessed as described before for AChR puncta. In the case of cells quantitative fluorescence analysis was performed as described previously (Hardel et al., 2008).

Confocal imaging

NMJs were imaged with a confocal scanning laser microscope (model SPE; Leica) using a HCX Plan Apochromat 100x objective (NA 1.46) and a resolution of 1024 × 1024 pixels. Quantitative differences potentially due to changes in the light source or camera were excluded by imaging control and mutant muscles within the same session.

Quantitative analysis of perforations

The percentage of perforated synapses was determined by calculating the fraction of NMJs in age-matched wild-type and mutant sternomastoid muscle that contained at least one "hole" or "perforation", defined as a region within the synaptic AChR cluster lacking α-BTX binding, but covered by nerve terminal.

Preparation of primary muscle cultures

Neonatal leg muscles from wild-type and mutant neonatal muscle were minced, dissociated with collagenase type IV and dispase type II, and cells were plated on a laminin substrate in DME containing 2 mM glutamine, 20% FCS, and 1% antibiotic/antimycotic solution. After 2 d, they were resuspended in PBS by brief trypsinization, treated with rat monoclonal anti–mouse α7-integrin antibody (a gift from R. Kremer, University of California, San Francisco, San Francisco, CA), and purified using (magnetic) Dynabeads coated with sheep anti–rat IgG and a Dynal-MPC-L magnetic particle concentrator (Blanco-Bose et al., 2001). C2C12, wild-type, or α-*db*$^{-/-}$ myotubes were cultured on laminin-coated dishes focally impregnated with agrin. For the preparation of the focally impregnated dishes COS-1 cells, transfected with a plasmid coding for full-length chicken agrin, were seeded at a density of 7–20 × 10^3 cells per 30 mm laminin-coated culture dish. After 48 h, cells were extracted for 1 h in 2% Triton X-100 in PBS, followed by intensive washing (6–8x 1 h PBS) and myoblast seeding (Jones et al., 1996). Subsequent differentiation was in DME, 5% horse serum, and 1% antibiotic/antimycotic solution. For biochemical analysis of α-DB1 phosphorylation at agrin-induced AChR clusters, myoblasts were seeded on laminin substrates coated uniformly with recombinant agrin. Agrin was nickel-affinity column purified from supernatants of EBNA-HEK 293 cell cultures that had been transfected with a His-tagged agrin construct containing 95 kD of the C terminus and the 25-kD laminin-binding domain NtAc95agrin (a gift from M.A. Rüegg, University of Basel, Basel, Switzerland) of the N terminus of chick agrin and selected for stable expression. For biochemistry, 6-well dishes were coated with 10 µg/ml laminin (Invitrogen) followed by coating with 0.5 µg/ml agrin solution (37°C, 2 h) before cell plating. It should be noted that throughout the present paper, agrin was applied attached to the culture substrate rather than in solution to mimic the in vivo situation.

Differences in AChR removal from agrin-induced AChR clusters were estimated from cultures in which agrin was deposited locally on laminin. Unlike the uniform coating with agrin described above, this method produces locally confined agrin patches which, when contacting myotubes, induced locally confined AChR clusters. To avoid differences in cluster size due to varying transfection efficiencies (see following paragraph), only clusters in myotubes grown on the same batch of COS-1 cell transfections were compared, and cluster size was expressed relative to control values.

Quantitative analysis of AChR cluster size

To determine AChR removal in culture, agrin-induced AChR clusters in primary myotubes were stained fluorescently and incubated for 6 h at 37°C (to allow removal of fluorescent receptors). When the removal rate was monitored in the absence of the ligand (NRG), cells were preincubated for 12 h with α-NRG1 antibody (Escher et al., 2005; to suppress endogenous NRG signaling), stained as before, and incubated for 6 h at 37°C in the presence of either recombinant NRG1β or α-NRG1 antibody. Cells were imaged (20x objective, NA 0.7) in wide field, and cluster sizes after 6 h were determined by measuring the area of the remaining AChR fluorescence in ImageJ (National Institutes of Health).

In situ hybridization

Probes and experimental protocols were as described previously (Moore et al., 2001). In brief, cRNA probes used were derived from full-length

cDNA encoding rat AChR-subunits or from cloned cDNA fragments encoding the extracellular domain of rat MuSK (Met-1 to Ser-435). Synaptic AChR clusters were localized by staining with α-BTX–Alexa 594 in 14-µm-thick frozen sections and hybridized with ^{35}S-labeled cRNA. PFA (4%)-fixed sections were treated with proteinase K (20 µg/ml in 50 mM TrisHCl/5 mM EDTA) for 8.5 min at room temperature, incubated for 10 min in 2.5% acetic anhydride in 0.1 M triethanolamine (pH 7.5), dehydrated through graded ethanol, and prehybridized for 3 h in hybridization buffer at 50°C. They were then hybridized overnight at 50°C with cRNA probes containing ^{35}S-labeled CTP and UTP (GE Healthcare) by using riboprobe concentrations between 40,000 and 180,000 cpm μl^{-1}. After washing with sodium-Tris-EDTA (NTE) buffer, sections were treated with 20 µg/ml RNase A for 45 min at 37°C and subsequently washed with increasing stringency (NTE and 2× sodium-sodium citrate [SSC] buffer at 37°C/0.1 × SSC at 50°C). After ethanol dehydration, they were dipped in Kodak NTB2 emulsion and exposed for 5–7 wk at 4°C.

Electron microscopy

Mice were perfused with 2.5% glutaraldehyde in 0.1 M sodium phosphate, pH 7.4, and muscles were post-fixed overnight at 4°C. Muscle pieces containing endplate regions were treated with 1% OsO_4 in 0.1 M cacodylate buffer, pH 7.2, rinsed in 1% Na_2SO_4 in 0.1 M cacodylate buffer, and embedded in Epon. Thin sections were post-stained with uranyl acetate and lead citrate, and were examined with an electron microscope (model EM400; Philips). The numbers of folds per µm of synaptic contact length was determined from prints.

Immunoaffinity purification and immunoblotting of protein complexes

To inhibit tyrosine phosphatases, peroxivanadate was prepared as described previously (Nawrotzki et al., 1998). In brief, sodium peroxivanadate was prepared fresh each time, just before use, by mixing 100 µl of 100 mM sodium orthovanadate and 200 µl of 100 mM H_2O_2 and then by adding 9.7 ml of prewarmed (37°C) serum-free medium. Peroxivanadate, ErbB inhibitors AG879 and AG1478 (5 µM) as well as NRG1-β (5 nM) were applied in serum-free DME (37°C, 30 min).

Myotubes from six wells were harvested in 300 µl of lysis buffer and protein complexes were purified as described previously (Kramarcy et al., 1994). In brief, myotubes harvested in ice-cold lysis buffer (10 mM Na_3PO_4, pH 7.8, 150 mM NaCl, 5 mM EDTA, 1 mM EGTA, 1% Triton X-100, protease inhibitor mixture [Roche], and phosphatase inhibitors Pic1 and Pic2 [Sigma-Aldrich]) were homogenized in a Dounce homogenizer and incubated for 3 h at 4°C with protein G–coupled mouse monoclonal syntrophin antibody 1351 (a kind gift from S.C. Froehner and M. Adams, University of Washington, Seattle, WA) or rabbit anti–α-dystrobrevin antibody (a kind gift of D.J. Blake and R. Nawrotzki, University of Cardiff, Wales, UK). Beads were then washed in lysis buffer containing protease inhibitors but without Triton X-100, resuspended in SDS loading buffer, and denatured (94°C, 3 min) before loading on either an 8–15% gradient or 8% acrylamide/0.8% bis-acrylamide gels buffered with Tris-glycine.

Gels were transferred onto PVDF membranes (Millipore) and subject to ECL (Thermo Fisher Scientific) development after incubation with primary and secondary antibodies. Milk (3%) was used as a blocking reagent except for the anti-phosphotyrosine 4G10 antibody, for which 3% BSA was used. The following primary antibodies were used: mouse monoclonal anti-syntrophin 1351 culture supernatant (30 µl/6 wells of myotubes), rabbit anti-α syntrophin 259 (5 µg/ml for Westerns; a kind gift of Stanly C. Froehner), rabbit anti-α-dystrobrevin (1:1,000; a kind gift from Derek J. Blake), mouse anti-phosphotyrosine, clone 4G10 (Milipore), and mouse anti-utrophin monoclonal (1:300). Goat anti–mouse IgG-HRP and goat anti–rabbit IgG-HRP secondary antibodies (Santa Cruz Biotechnology, Inc.) were used at a 1:5,000 dilution.

Statistical analyses

Data are given as mean ± SEM. Quantitative comparisons of numerical datasets were tested for statistical significance by means of the nonparametric, two-sided *U* test (Mann & Whitney) with *, $P < 0.05$; **, $P < 0.01$; and ***, $P > 0.001$ unless stated otherwise. In the case of categorical datasets, χ^2 statistics were performed.

Online supplemental material

Figure S1 shows in situ hybridization of musk as well as achr α- and ε-subunit in wild-type and *erbb2/4*$^{-/-}$ muscle cross sections. Figure S2 demonstrates the inhibition of AChR internalization from perisynaptic sites by dynasore in vivo. Figure S3 shows the increase of perisynaptic recycled AChR puncta and streaks in wild-type NMJs treated with AG1478/AG879 (ErbB kinase inhibitors). Figure S4 illustrates that rapsyn and utrophin co-migrate with AChRs to perisynaptic sites and that this co-migration is accelerated in *erbb2/4*$^{-/-}$ NMJs. Figure S5 displays the full blot of the anti-syntrophin IP from C2C12 myotubes treated with AG879 or AG1478 compared with nontreated control. Blots were exposed to anti-α-DB1 and anti-phosphotyrosine (4G10) antibodies. Online supplemental material is available at http://www.jcb.org/cgi/content/full/jcb.201107083/DC1.

We are indebted to Clarke Slater and Richard Hume for critical comments on the manuscript. We thank the following colleagues for sharing various materials and tools as mentioned in the Materials and methods section: M. Adams, D. Blake, S. Froehner, R. Kremer, R. Levinson, M. Maimone, C. Mouslim, B. Pawlikowski, M.A. Rüegg, J.R. Sanes, and L. Sorokin. We thank U. Sauder from the Microscopy Center of the University of Basel for electron microscopy, and M. Courtet for myotube culturing. The anti-actin (JLA20), anti-utrophin, anti–β-dystroglycan, and anti-AChR (mab35) antibodies were obtained from the Developmental Studies Hybridoma Bank.

This work was supported by grants from the Swiss National Science Foundation, the Swiss Foundation for Research on Muscle Diseases, the Neuromuscular Research Association Basel (NeRAB), and the University of Basel (to H.R. Brenner), and from the National Institutes of Health and MDA (to M. Akaaboune).

Author contributions: M. Akaaboune and I. Martinez-Pena y Valenzuela performed in vivo imaging; N. Schmidt and M. Akaaboune performed in vivo experiments and confocal imaging; N. Gajendran conducted biochemical work and produced recombinant agrin; S. Wakefield did cell biology; R. Thurnheer and H.R. Brenner made contraction measurements; N. Gajendran and H.R. Brenner conducted in situ hybridization; and H.R. Brenner and M. Akaaboune designed and supervised the study and wrote the manuscript.

Submitted: 13 July 2011
Accepted: 18 November 2011

References

Adams, M.E., N. Kramarcy, S.P. Krall, S.G. Rossi, R.L. Rotundo, R. Sealock, and S.C. Froehner. 2000. Absence of alpha-syntrophin leads to structurally aberrant neuromuscular synapses deficient in utrophin. *J. Cell Biol.* 150:1385–1398. http://dx.doi.org/10.1083/jcb.150.6.1385

Akaaboune, M., S.M. Culican, S.G. Turney, and J.W. Lichtman. 1999. Rapid and reversible effects of activity on acetylcholine receptor density at the neuromuscular junction in vivo. *Science*. 286:503–507. http://dx.doi.org/10.1126/science.286.5439.503

Akaaboune, M., R.M. Grady, S. Turney, J.R. Sanes, and J.W. Lichtman. 2002. Neurotransmitter receptor dynamics studied in vivo by reversible photounbinding of fluorescent ligands. *Neuron*. 34:865–876. http://dx.doi.org/10.1016/S0896-6273(02)00739-0

Banks, G.B., C. Fuhrer, M.E. Adams, and S.C. Froehner. 2003. The postsynaptic submembrane machinery at the neuromuscular junction: requirement for rapsyn and the utrophin/dystrophin-associated complex. *J. Neurocytol.* 32:709–726. http://dx.doi.org/10.1023/B:NEUR.0000020619.24681.2b

Bao, J., D. Wolpowitz, L.W. Role, and D.A. Talmage. 2003. Back signaling by the Nrg-1 intracellular domain. *J. Cell Biol.* 161:1133–1141. http://dx.doi.org/10.1083/jcb.200212085

Blanco-Bose, W.E., C.C. Yao, R.H. Kramer, and H.M. Blau. 2001. Purification of mouse primary myoblasts based on alpha 7 integrin expression. *Exp. Cell Res.* 265:212–220. http://dx.doi.org/10.1006/excr.2001.5191

Bruneau, E.G., and M. Akaaboune. 2006. The dynamics of recycled acetylcholine receptors at the neuromuscular junction in vivo. *Development*. 133:4485–4493. http://dx.doi.org/10.1242/dev.02619

Bruneau, E., D. Sutter, R.I. Hume, and M. Akaaboune. 2005a. Identification of nicotinic acetylcholine receptor recycling and its role in maintaining receptor density at the neuromuscular junction in vivo. *J. Neurosci.* 25:9949–9959. http://dx.doi.org/10.1523/JNEUROSCI.3169-05.2005

Bruneau, E.G., P.C. Macpherson, D. Goldman, R.I. Hume, and M. Akaaboune. 2005b. The effect of agrin and laminin on acetylcholine receptor dynamics in vitro. *Dev. Biol.* 288:248–258. http://dx.doi.org/10.1016/j.ydbio.2005.09.041

Bruneau, E.G., D.S. Brenner, J.Y. Kuwada, and M. Akaaboune. 2008. Acetylcholine receptor clustering is required for the accumulation and maintenance of scaffolding proteins. *Curr. Biol.* 18:109–115. http://dx.doi.org/10.1016/j.cub.2007.12.029

Bruneau, E.G., J.A. Esteban, and M. Akaaboune. 2009. Receptor-associated proteins and synaptic plasticity. *FASEB J.* 23:679–688. http://dx.doi.org/10.1096/fj.08-107946

Deconinck, A.E., A.C. Potter, J.M. Tinsley, S.J. Wood, R. Vater, C. Young, L. Metzinger, A. Vincent, C.R. Slater, and K.E. Davies. 1997a. Postsynaptic abnormalities at the neuromuscular junctions of utrophin-deficient mice. *J. Cell Biol.* 136:883–894. http://dx.doi.org/10.1083/jcb.136.4.883

Deconinck, A.E., J.A. Rafael, J.A. Skinner, S.C. Brown, A.C. Potter, L. Metzinger, D.J. Watt, J.G. Dickson, J.M. Tinsley, and K.E. Davies. 1997b. Utrophin-dystrophin-deficient mice as a model for Duchenne muscular dystrophy. *Cell*. 90:717–727. http://dx.doi.org/10.1016/S0092-8674(00)80532-2

Delbono, O., J. Xia, S. Treves, Z.M. Wang, R. Jimenez-Moreno, A.M. Payne, M.L. Messi, A. Briguet, F. Schaerer, M. Nishi, et al. 2007. Loss of skeletal muscle strength by ablation of the sarcoplasmic reticulum protein JP45. *Proc. Natl. Acad. Sci. USA*. 104:20108–20113. http://dx.doi.org/10.1073/pnas.0707389104

Escher, P., E. Lacazette, M. Courtet, A. Blindenbacher, L. Landmann, G. Bezakova, K.C. Lloyd, U. Mueller, and H.R. Brenner. 2005. Synapses form in skeletal muscles lacking neuregulin receptors. *Science*. 308:1920–1923. http://dx.doi.org/10.1126/science.1108258

Froehner, S.C., A.A. Murnane, M. Tobler, H.B. Peng, and R. Sealock. 1987. A postsynaptic Mr 58,000 (58K) protein concentrated at acetylcholine receptor-rich sites in Torpedo electroplaques and skeletal muscle. *J. Cell Biol.* 104:1633–1646. http://dx.doi.org/10.1083/jcb.104.6.1633

Fukazawa, R., T.A. Miller, Y. Kuramochi, S. Frantz, Y.D. Kim, M.A. Marchionni, R.A. Kelly, and D.B. Sawyer. 2003. Neuregulin-1 protects ventricular myocytes from anthracycline-induced apoptosis via erbB4-dependent activation of PI3-kinase/Akt. *J. Mol. Cell. Cardiol.* 35:1473–1479. http://dx.doi.org/10.1016/j.yjmcc.2003.09.012

Grady, R.M., J.P. Merlie, and J.R. Sanes. 1997. Subtle neuromuscular defects in utrophin-deficient mice. *J. Cell Biol.* 136:871–882. http://dx.doi.org/10.1083/jcb.136.4.871

Grady, R.M., R.W. Grange, K.S. Lau, M.M. Maimone, M.C. Nichol, J.T. Stull, and J.R. Sanes. 1999. Role for alpha-dystrobrevin in the pathogenesis of dystrophin-dependent muscular dystrophies. *Nat. Cell Biol.* 1:215–220. http://dx.doi.org/10.1038/12034

Grady, R.M., H. Zhou, J.M. Cunningham, M.D. Henry, K.P. Campbell, and J.R. Sanes. 2000. Maturation and maintenance of the neuromuscular synapse: genetic evidence for roles of the dystrophin—glycoprotein complex. *Neuron*. 25:279–293. http://dx.doi.org/10.1016/S0896-6273(00)80894-6

Grady, R.M., M. Akaaboune, A.L. Cohen, M.M. Maimone, J.W. Lichtman, and J.R. Sanes. 2003. Tyrosine-phosphorylated and nonphosphorylated isoforms of alpha-dystrobrevin: roles in skeletal muscle and its neuromuscular and myotendinous junctions. *J. Cell Biol.* 160:741–752. http://dx.doi.org/10.1083/jcb.200209045

Hardel, N., N. Harmel, G. Zolles, B. Fakler, and N. Klöcker. 2008. Recycling endosomes supply cardiac pacemaker channels for regulated surface expression. *Cardiovasc. Res.* 79:52–60. http://dx.doi.org/10.1093/cvr/cvn062

Jacobson, C., P.D. Côté, S.G. Rossi, R.L. Rotundo, and S. Carbonetto. 2001. The dystroglycan complex is necessary for stabilization of acetylcholine receptor clusters at neuromuscular junctions and formation of the synaptic basement membrane. *J. Cell Biol.* 152:435–450. http://dx.doi.org/10.1083/jcb.152.3.435

Jones, G., A. Herczeg, M.A. Ruegg, M. Lichtsteiner, S. Kröger, and H.R. Brenner. 1996. Substrate-bound agrin induces expression of acetylcholine receptor epsilon-subunit gene in cultured mammalian muscle cells. *Proc. Natl. Acad. Sci. USA*. 93:5985–5990. http://dx.doi.org/10.1073/pnas.93.12.5985

Jones, G., C. Moore, S. Hashemolhosseini, and H.R. Brenner. 1999. Constitutively active MuSK is clustered in the absence of agrin and induces ectopic postsynaptic-like membranes in skeletal muscle fibers. *J. Neurosci.* 19:3376–3383.

Kramarcy, N.R., A. Vidal, S.C. Froehner, and R. Sealock. 1994. Association of utrophin and multiple dystrophin short forms with the mammalian M(r) 58,000 dystrophin-associated protein (syntrophin). *J. Biol. Chem.* 269:2870–2876.

Krejci, E., I. Martinez-Pena y Valenzuela, R. Ameziane, and M. Akaaboune. 2006. Acetylcholinesterase dynamics at the neuromuscular junction of live animals. *J. Biol. Chem.* 281:10347–10354. http://dx.doi.org/10.1074/jbc.M507502200

Lacazette, E., S. Le Calvez, N. Gajendran, and H.R. Brenner. 2003. A novel pathway for MuSK to induce key genes in neuromuscular synapse formation. *J. Cell Biol.* 161:727–736. http://dx.doi.org/10.1083/jcb.200210156

Leu, M., E. Bellmunt, M. Schwander, I. Fariñas, H.R. Brenner, and U. Müller. 2003. Erbb2 regulates neuromuscular synapse formation and is essential for muscle spindle development. *Development*. 130:2291–2301. http://dx.doi.org/10.1242/dev.00447

Levitzki, A., and A. Gazit. 1995. Tyrosine kinase inhibition: an approach to drug development. *Science*. 267:1782–1788. http://dx.doi.org/10.1126/science.7892601

Martinez-Pena y Valenzuela, I., and M. Akaaboune. 2007. Acetylcholinesterase mobility and stability at the neuromuscular junction of living mice. *Mol. Biol. Cell*. 18:2904–2911. http://dx.doi.org/10.1091/mbc.E07-02-0093

Martinez-Pena y Valenzuela, I., R.I. Hume, E. Krejci, and M. Akaaboune. 2005. In vivo regulation of acetylcholinesterase insertion at the neuromuscular junction. *J. Biol. Chem.* 280:31801–31808. http://dx.doi.org/10.1074/jbc.M502874200

Mei, L., and W.C. Xiong. 2008. Neuregulin 1 in neural development, synaptic plasticity and schizophrenia. *Nat. Rev. Neurosci.* 9:437–452. http://dx.doi.org/10.1038/nrn2392

Meier, T., F. Masciulli, C. Moore, F. Schoumacher, U. Eppenberger, A.J. Denzer, G. Jones, and H.R. Brenner. 1998. Agrin can mediate acetylcholine receptor gene expression in muscle by aggregation of muscle-derived neuregulins. *J. Cell Biol.* 141:715–726. http://dx.doi.org/10.1083/jcb.141.3.715

Moore, C., M. Leu, U. Müller, and H.R. Brenner. 2001. Induction of multiple signaling loops by MuSK during neuromuscular synapse formation. *Proc. Natl. Acad. Sci. USA*. 98:14655–14660. http://dx.doi.org/10.1073/pnas.251291598

Nawrotzki, R., N.Y. Loh, M.A. Ruegg, K.E. Davies, and D.J. Blake. 1998. Characterisation of alpha-dystrobrevin in muscle. *J. Cell Sci.* 111:2595–2605.

Patton, B.L., J.M. Cunningham, J. Thyboll, J. Kortesmaa, H. Westerblad, L. Edström, K. Tryggvason, and J.R. Sanes. 2001. Properly formed but improperly localized synaptic specializations in the absence of laminin alpha4. *Nat. Neurosci.* 4:597–604. http://dx.doi.org/10.1038/88414

Pawlikowski, B.T., and M.M. Maimone. 2009. Formation of complex AChR aggregates in vitro requires alpha-dystrobrevin. *Dev. Neurobiol.* 69:326–338. http://dx.doi.org/10.1002/dneu.20703

Peng, H.B., H. Xie, S.G. Rossi, and R.L. Rotundo. 1999. Acetylcholinesterase clustering at the neuromuscular junction involves perlecan and dystroglycan. *J. Cell Biol.* 145:911–921. http://dx.doi.org/10.1083/jcb.145.4.911

Pennefather, P., and D.M. Quastel. 1981. Relation between subsynaptic receptor blockade and response to quantal transmitter at the mouse neuromuscular junction. *J. Gen. Physiol.* 78:313–344. http://dx.doi.org/10.1085/jgp.78.3.313

Sandrock, A.W. Jr., S.E. Dryer, K.M. Rosen, S.N. Gozani, R. Kramer, L.E. Theill, and G.D. Fischbach. 1997. Maintenance of acetylcholine receptor number by neuregulins at the neuromuscular junction in vivo. *Science*. 276:599–603. http://dx.doi.org/10.1126/science.276.5312.599

Schaeffer, L., A. de Kerchove d'Exaerde, and J.P. Changeux. 2001. Targeting transcription to the neuromuscular synapse. *Neuron*. 31:15–22. http://dx.doi.org/10.1016/S0896-6273(01)00353-1

Slater, C.R. 2008. Structural factors influencing the efficacy of neuromuscular transmission. *Ann. N. Y. Acad. Sci.* 1132:1–12. http://dx.doi.org/10.1196/annals.1405.003

Sunderland, W.J., Y.J. Son, J.H. Miner, J.R. Sanes, and S.S. Carlson. 2000. The presynaptic calcium channel is part of a transmembrane complex linking a synaptic laminin (alpha4beta2gamma1) with non-erythroid spectrin. *J. Neurosci.* 20:1009–1019.

Turney, S.G., S.M. Culican, and J.W. Lichtman. 1996. A quantitative fluorescence-imaging technique for studying acetylcholine receptor turnover at neuromuscular junctions in living animals. *J. Neurosci. Methods*. 64:199–208. http://dx.doi.org/10.1016/0165-0270(95)00135-2

Valdez, G., J.C. Tapia, H. Kang, G.D. Clemenson Jr., F.H. Gage, J.W. Lichtman, and J.R. Sanes. 2010. Attenuation of age-related changes in mouse neuromuscular synapses by caloric restriction and exercise. *Proc. Natl. Acad. Sci. USA*. 107:14863–14868. http://dx.doi.org/10.1073/pnas.1002220107

Waite, A., C.L. Tinsley, M. Locke, and D.J. Blake. 2009. The neurobiology of the dystrophin-associated glycoprotein complex. *Ann. Med.* 41:344–359. http://dx.doi.org/10.1080/07853890802668522

Witzemann, V., H. Schwarz, M. Koenen, C. Berberich, A. Villarroel, A. Wernig, H.R. Brenner, and B. Sakmann. 1996. Acetylcholine receptor epsilon-subunit deletion causes muscle weakness and atrophy in juvenile and adult mice. *Proc. Natl. Acad. Sci. USA*. 93:13286–13291. http://dx.doi.org/10.1073/pnas.93.23.13286

Woo, R.S., X.M. Li, Y. Tao, E. Carpenter-Hyland, Y.Z. Huang, J. Weber, H. Neiswender, X.P. Dong, J. Wu, M. Gassmann, et al. 2007. Neuregulin-1 enhances depolarization-induced GABA release. *Neuron*. 54:599–610. http://dx.doi.org/10.1016/j.neuron.2007.04.009

Wood, S.J., and C.R. Slater. 1997. The contribution of postsynaptic folds to the safety factor for neuromuscular transmission in rat fast- and slow-twitch muscles. *J. Physiol.* 500:165–176.